Article

Cultivation and visualization of a methanogen of the phylum Thermoproteota

https://doi.org/10.1038/s41586-024-07631-6

Received: 20 January 2023

Accepted: 30 May 2024

Published online: 24 July 2024

Check for updates

Anthony J. Kohtz[1], Nikolai Petrosian[2,4], Viola Krukenberg[1,4], Zackary J. Jay[1,4], Martin Pilhofer[2] & Roland Hatzenpichler[1,3]✉

Methane is the second most abundant climate-active gas, and understanding its sources and sinks is an important endeavour in microbiology, biogeochemistry, and climate sciences[1,2]. For decades, it was thought that methanogenesis, the ability to conserve energy coupled to methane production, was taxonomically restricted to a metabolically specialized group of archaea, the Euryarchaeota[1]. The discovery of marker genes for anaerobic alkane cycling in metagenome-assembled genomes obtained from diverse habitats has led to the hypothesis that archaeal lineages outside the Euryarchaeota are also involved in methanogenesis[3–6]. Here we cultured *Candidatus* Methanosuratincola verstraetei strain LCB70, a member of the archaeal class Methanomethylicia (formerly Verstraetearchaeota) within the phylum Thermoproteota, from a terrestrial hot spring. Growth experiments combined with activity assays, stable isotope tracing, and genomic and transcriptomic analyses demonstrated that this thermophilic archaeon grows by means of methyl-reducing hydrogenotrophic methanogenesis. Cryo-electron tomography revealed that *Ca*. M. verstraetei are coccoid cells with archaella and chemoreceptor arrays, and that they can form intercellular bridges connecting two to three cells with continuous cytoplasm and S-layer. The wide environmental distribution of *Ca*. M. verstraetei suggests that they might play important and hitherto overlooked roles in carbon cycling within diverse anoxic habitats.

Methanogens, strictly anaerobic archaea that conserve energy coupled to methane production, are responsible for approximately two-thirds of global methane emissions (576 Tg per year)[7,8]. Methanogens can exploit carbon dioxide, hydrogen and a variety of organic compounds, such as formate, acetate, or methylated or methoxylated molecules, to fuel their growth[2]. All methanogenic pathways require methyl-coenzyme M reductase (MCR), the enzyme complex catalysing the conversion of methyl-coenzyme M (CH_3-CoM) and coenzyme B (CoB) into methane and a heterodisulfide (CoM-S-S-CoB)[9]. Because of its importance in all known methanogenic pathways and in the anaerobic oxidation of hydrocarbons, MCR-encoding genes are commonly used to identify potential alkane cycling archaea[2,10]. Methanogens have been cultured since the early 1900s[11] but to date all belong to the superphylum Euryarchaeota[12].

The discovery of *mcr* and other methanogenesis marker genes in diverse metagenome-assembled genomes (MAGs) has led to the proposal that several lineages within the archaeal phyla Asgardarchaeota, Hadarchaeota, and Thermoproteota (formerly the TACK superphylum) might engage in anaerobic alkane cycling[3–6,13,14]. In contrast to most cultured methanogens that conserve energy exclusively by means of methanogenesis, many of these MCR-encoding MAGs encode alternative energy-conserving pathways, such as dissimilatory sulfite reduction[3,14] or fermentation[5,6]. The potential of these MCR-encoding archaea to switch their growth modality depending on environmental conditions might provide them an advantage over obligate methanogens. However, so far, no methanogen from outside the Euryarchaeota has been cultured or visualized, and no experimental evidence exists to support metagenome-based metabolic predictions.

Here we combined cultivation, microscopy, metagenomics and metatranscriptomics, growth experiments, stable isotope tracing and single-cell activity assays to demonstrate that a member of the phylum Thermoproteota is a methyl-reducing hydrogenotrophic methanogen. Furthermore, we visualized the morphology and unique ultrastructure of a methanogen outside the Euryarchaeota by fluorescence microscopy and cryo-electron tomography (cryo-ET).

Cultivation of a novel methanogen

Geothermal features, such as hot springs, have recently been shown to harbour a wide diversity of MCR-encoding archaea[3,4,14–20], which makes them promising sources for targeted cultivation of these microorganisms. In a recent survey of geothermal features in Yellowstone National Park (YNP), we identified the Lower Culex Basin (LCB) as an area with strong potential for methanogenesis[17]. From the sediment metagenome of hot spring LCB070, we reconstructed two MAGs affiliated with the class Methanomethylicia (formerly Verstraetearchaeota[6])

[1]Department of Chemistry and Biochemistry, Center for Biofilm Engineering, and Thermal Biology Institute, Montana State University, Bozeman, MT, USA. [2]Institute of Molecular Biology and Biophysics, ETH Zürich, Zürich, Switzerland. [3]Department of Microbiology and Cell Biology, Montana State University, Bozeman, MT, USA. [4]These authors contributed equally: Nikolai Petrosian, Viola Krukenberg, Zackary J. Jay. ✉e-mail: roland.hatzenpichler@montana.edu

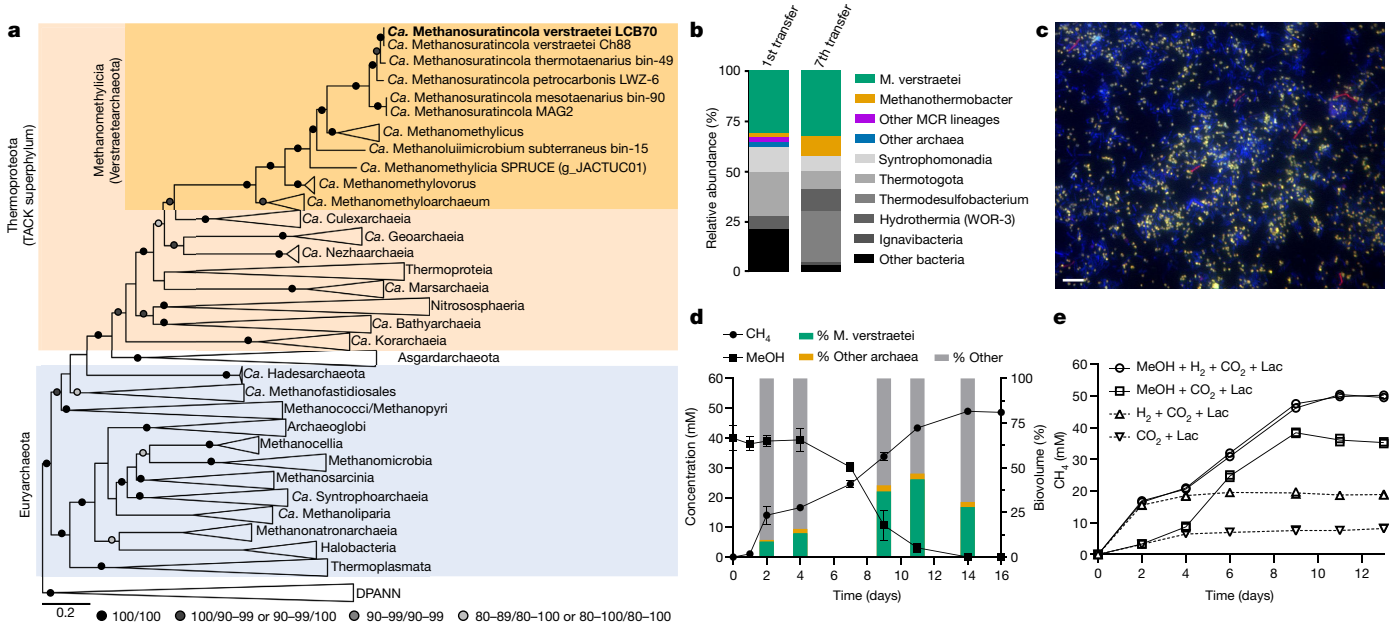

Fig. 1 | Characterization of the methanogenic enrichment culture. **a**, Phylogenomic tree of archaea based on a set of 33 single-copy marker genes, with *Ca*. M. verstraetei LCB70 in bold. Circles at the nodes indicate the ranges for the SH-like approximate-likelihood ratio test and ultrafast bootstrap support, respectively, and only values above 80 are shown. **b**, Community composition of the culture at the first transfer based on the relative abundance of the LCB70 genome and other MAGs recovered from metagenome sequencing and at the seventh transfer based on 16S rRNA gene amplicon sequencing. **c**, Visualization of the culture by 16S rRNA-targeted FISH. M. verstraetei cells in yellow (dual labelled by the Methanomethyliaceae-specific probe Msur657 and the general archaeal probe Arch915), other archaeal cells in red (labelled by Arch915). The DAPI-stained cells not hybridized with either probe in blue. Scale bar, 5 µm. A representative image of $n = 3$ independent samples from one culture is shown. **d**, Growth curve depicting methane production, methanol depletion and relative abundance of LCB70 and other archaea (%) over time as determined with FISH. Data for methane and methanol (MeOH) are the mean ($n = 4$ biological replicates) ± s.d. and % biovolume is the mean ($n = 4$ biological replicates). Where not visible, the error bars are smaller than the symbol. **e**, Methane production by the culture under different substrate amendments. The line represents the mean and symbols show values for each replicate ($n = 2$ biological replicates). Methane production in incubations without methanol is due to the activity of *Methanothermobacter*. When methanol, a substrate that *Methanothermobacter* cannot use, is present LCB70 converts it into methane by means of methyl-reducing methanogenesis.

within the phylum Thermoproteota[12] (Extended Data Fig. 1). Consistent with Methanomethylicia MAGs previously obtained from other habitats[3,6,16,21], the two MAGs from LCB070 encode the potential for methyl-reducing hydrogenotrophic methanogenesis[2].

Using a sediment–water slurry from hot spring LCB070 as inoculum, we initiated a methanogenic culture supplied with methanol and hydrogen in anoxic media (64 °C, pH 6.5). After one transfer, fluorescence in situ hybridization (FISH) with a newly designed Methanomethyliaceae-specific 16S rRNA-targeted probe detected an abundant population of coccoid cells. Metagenomic sequencing showed that the most abundant organism was an MCR-encoding member of the Methanomethylicia (31.4% relative abundance; Supplementary Table 1).

Using a combination of Illumina short-read and Nanopore long-read sequencing, we assembled the complete circular genome of this archaeon, which had a size of 1.52 Mb and a GC content of 54.6% (Supplementary Table 1). 16S rRNA gene and single-copy marker protein phylogenies placed the archaeon within the phylum Thermoproteota (Fig. 1a). Comparative amino acid, nucleotide, and 16S rRNA gene sequence identity analyses further classified the genome within the genus *Candidatus* Methanosuratincola[6,22] (Extended Data Fig. 2). We propose to name this archaeon *Ca*. M. verstraetei strain LCB70 (see 'Etymology' in Supplementary Information). Interestingly, LCB70 was not closely related to the two MAGs recovered from the original hot spring metagenome (Extended Data Figs. 1 and 2), suggesting that it represented a low abundance population in feature LCB070 at the time of sampling. Analysis of *Ca*. M. verstraetei-related 16S rRNA gene sequences in public databases revealed that they are present in a variety of anoxic habitats, including bioreactors, freshwater and marine sediments, hot springs, hydrocarbon reservoirs, soils, rumen and wastewater sludge (Extended Data Fig. 3 and Supplementary Table 2). This demonstrates that methanogens within this group might contribute to methane cycling in ecosystems other than hot springs.

By the seventh transfer we had obtained a sediment-free methanogenic culture, in which LCB70 (32.8% relative abundance) and *Methanothermobacter* spp. (9.7% relative abundance) were the only archaeal populations detectable by 16S rRNA gene amplicon sequencing (Fig. 1b). Based on FISH with the LCB70-specific and general archaeal probes, the two populations were distinguished by their coccoid (LCB70) and filamentous (*Methanothermobacter* spp.) morphologies (Fig. 1c). Thus, we established a stable mixed culture of LCB70, a proposed methyl-reducing methanogen and *Methanothermobacter* spp., obligate carbon dioxide-reducing methanogens[23–25]. Furthermore, we found that methane production and growth of the culture improved when supplemented with an additional carbon source (lactate, acetate or pyruvate; Extended Data Fig. 4).

LCB70 converts methanol to methane

In cultures supplied with methanol, hydrogen and lactate, the relative abundance of LCB70 increased alongside methane production and methanol depletion (Fig. 1d). The biovolume fraction of LCB70 in the culture determined with FISH increased from an average of 8.7% in the lag phase to up to 43.5% during the log phase of methane production (Fig. 1d). In the stationary phase, when methanol had been depleted and methane production ceased, the biovolume fraction of LCB70 decreased to 28%, probably due to substrate starvation (Fig. 1d). When methanol was omitted, methane production was strongly reduced and

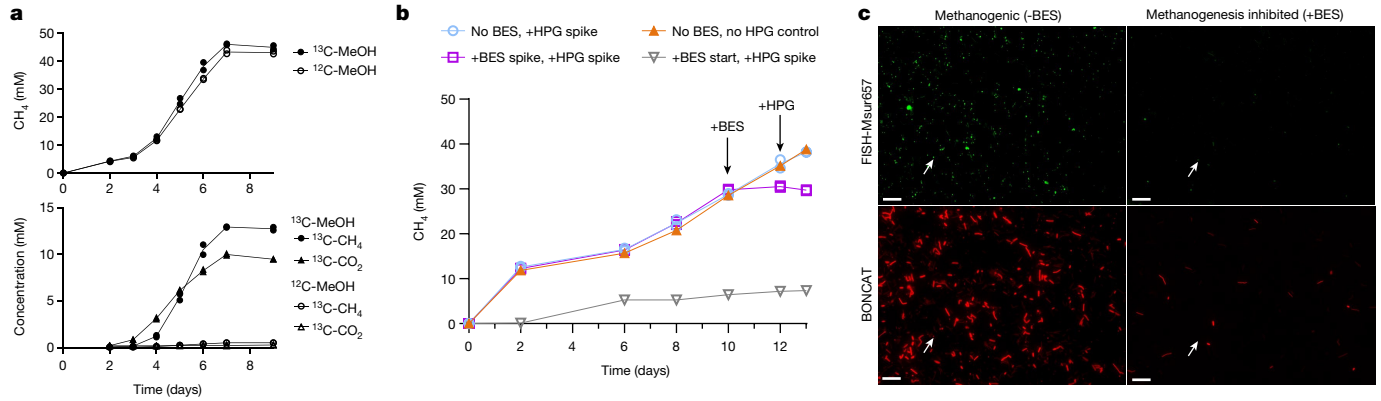

Fig. 2 | Translational activity and conversion of stable isotope tracers. **a**, Incubation experiments with ^{13}C-methanol (25 mM ^{13}C-methanol and 25 mM ^{12}C-methanol; closed symbols) and ^{12}C-methanol (50 mM added) as control (open symbols). Top, total methane produced over time. Bottom, ^{13}C-methane (circles) and ^{13}C-carbon dioxide (triangles) produced over time. The line represents the mean and symbols show values for each replicate ($n = 2$ biological replicates). **b**, Methane production in incubations for BONCAT and FISH (BONCAT–FISH) experiments ($n = 2$ biological replicates for No BES + HPG spike and +BES spike +HPG spike; $n = 1$ biological replicate for No HPG control and +BES start). The line represents the mean and symbols show values for each replicate. Arrows indicate BES and HPG addition. Methane production stops upon BES addition on day 10. **c**, The LCB70 cells detected with FISH (green) and translationally active cells detected with BONCAT (red). Under methanogenic conditions, LCB70 cells were translationally active. When methanogenesis was inhibited by BES, LCB70 cells were inactive. White arrows indicate examples of LCB70 cells. Note that the relative fluorescence intensity of LCB70 as compared with other cells is non-informative in BONCAT experiments[28]. Representative images from $n = 3$ independent samples from $n = 2$ biological replicate cultures are shown.

growth of LCB70 could not be sustained (Fig. 1e). The biovolume of *Methanothermobacter* ranged from 0.9% to 3.4% between days 2 and 11 (Fig. 1d). In the first two to four days of the culture, methane production is not coupled to methanol depletion and LCB70 is of comparatively low abundance. By contrast, during later stages of the culture, when methane production is coupled to methanol depletion, LCB70 is most abundant, further indicating the reliance of LCB70 on methanol (Fig. 1d).

The two methanogen populations, LCB70 and *Methanothermobacter*, use different pathways for methanogenesis. The LCB70 encodes genes for methyl-reducing hydrogenotrophic methanogenesis but lacks genes for carbon dioxide-reducing hydrogenotrophic or acetoclastic methanogenesis. By contrast, *Methanothermobacter* are obligate hydrogen- and carbon dioxide-utilizing methanogens which lack methyltransferase genes[23,24]. To determine the contribution to methane production by the two methanogens, we further incubated the culture under conditions with and without methanol and hydrogen (Fig. 1e). Total methane production in cultures without methanol was greatly reduced and was due to the activity of the carbon dioxide-utilizing *Methanothermobacter*. When methanol, a substrate that *Methanothermobacter* cannot use, was present, LCB70 contributed to methane production by converting methanol into methane by means of methyl-reducing hydrogenotrophic methanogenesis. When hydrogen was not supplied, methane production occurred, which indicates that hydrogen-producing organisms coexist with methanogens in the culture (Fig. 1e). We conducted a stable isotope tracer experiment, in which a culture grown in the absence of hydrogen was incubated in the presence of ^{13}C-methanol. We observed that 52% of the added ^{13}C-methanol was converted to ^{13}C-methane and that 40% was converted to ^{13}C-carbon dioxide (Fig. 2c). The production of ^{13}C-carbon dioxide suggests that other organisms in the culture also metabolize methanol. Consistently, methanol-oxidizing bacteria affiliated with Syntrophomonadia (7%–12% relative abundance) and Thermotogota (8%–21% relative abundance) that expressed methanol methyltransferases and methanol dehydrogenases, respectively, were co-enriched in the culture (Fig. 1b and Supplementary Table 3). Further, we hypothesize that these methanol-degraders in the culture probably form carbon dioxide, hydrogen and acetate, and engage in a syntrophic interaction with consumers of these byproducts, including LCB70 and *Methanothermobacter*, as observed in other thermophilic, methanogenic co-cultures and bioreactors[26,27]. In future studies, ^{13}C- and ^{2}H-labelling experiments performed under different physicochemical conditions might help to reconcile these ideas.

To study the metabolic activity of LCB70 under methanogenic and methanogenesis-inhibited conditions, we performed bioorthogonal non-canonical amino acid tagging (BONCAT) incubations to label translationally active cells[28,29]. For this, replicate cultures grown to the exponential phase of methane production were spiked with 2-bromoethanesulfonate (BES), an inhibitor of the MCR complex (Fig. 2b). After a 48 h incubation, L-homopropargylglycine (HPG), a tracer of translational activity, was added to BES-amended cultures and to controls without BES. After 24 h of incubation with HPG, we analysed cells by BONCAT–FISH to directly link taxonomic identity and translational activity at a single-cell level. We observed active LCB70 cells under methanogenic conditions, but not under methanogenesis-inhibited conditions (absence of BES; Fig. 2c). This indicates that translational activity and subsequent energy conservation in LCB70 relies on the functional operation of the MCR complex, and thus methanogenesis.

Metabolic potential and gene expression

Recovery of the complete circular genome of strain LCB70 enabled us to reconstruct its metabolic potential and analyse its gene expression when grown on methanol, hydrogen and lactate. Consistent with methanol-dependent methane production in the culture, strain LCB70 encodes the potential for methyl-reducing hydrogenotrophic methanogenesis. Strain LCB70 highly expressed the methanol-specific methyltransferase system and the MCR complex, enabling the conversion of methanol to CoM-S-S-CoB and methane (Fig. 3a,b). Strain LCB70 also encodes two copies of another methyltransferase, MtmB, which could be involved in converting monomethylamine to methane, and these genes were expressed at about 1% of the rate of MtaB (Fig. 3b). However, in contrast to the close relative *Ca*. M. petrocarbonis LWZ-6, which uses monomethylamine[30], attempts to grow strain LCB70 on monomethylamine have so far been unsuccessful. Furthermore, strain LCB70 lacks the tetrahydromethanopterin *S*-methyltransferase complex and methyl branch of the Wood–Ljungdahl pathway, indicating it is not able to oxidize methanol to carbon dioxide, which would be required for a methyl-dismutating methanogenesis pathway[2]. Additionally, we observed that expression of the methanogenesis and energy conservation pathways was largely similar across cultures grown with lactate as

compared with those grown with pyruvate or acetate as carbon sources (Extended Data Fig. 4 and Supplementary Table 4).

Beyond methyltransferases and the MCR complex, LCB70 also encodes several complexes involved in the reduction of CoM-S-S-CoB, energy conservation, and hydrogen metabolism. The proposed HdrBC-interacting [NiFe]-hydrogenase complex, Ehd, was the highest expressed hydrogenase and could couple the oxidation of hydrogen to the reduction of CoM-S-S-CoB and translocation of H^+ or Na^+ across the membrane[3,31]. Strain LCB70 also expressed a group 4i [NiFe]-hydrogenase, Ehb. In other methanogens, Ehb has been implicated in several processes, including energy conservation and hydrogen production in *Methanosphaera stadtmanae*, and providing reduced ferredoxins for anabolism in *Methanococcus maripaludis*[1,32]. Thus, additional physiology studies are required to deduce the function and regulation of Ehb in strain LCB70. Additionally, a cytoplasmic group 3b [NiFe]-hydrogenase that belongs to the group of potential sulfydrogenases was lowly expressed. This enzyme catalyses the reversible oxidation of NADPH coupled to the reduction of protons or sulfur (S^0) to hydrogen or hydrogen sulfide and may be important under yet-unknown growth conditions[33].

Notably, in contrast to previous findings based on Methanomethylicia MAGs[6,16], we did not identify genes encoding an Fpo-like complex in the LCB70 genome. However, LCB70 expresses a novel group 4g [NiFe] hydrogenase, termed Ehi here, which is also present in diverse Thermoproteota lineages (Fig. 3 and Extended Data Fig. 5). This Ehi complex shares similarities to Fpo-like complexes in archaea, including the same 11-subunit organization. However, the catalytic subunit has conserved motifs (CxxC) at the N and C-termini for coordination of a [NiFe] cofactor, which are absent in Fpo–Nuo complexes[34,35]. Therefore, we suggest that Ehi could functionally substitute for a Fpo-like complex in LCB70. If Ehi formed a complex with heterodisulfide reductase (HdrD), in a similar fashion to the Fpo–HdrD complex in Methanomassiliicoccales[34,36,37], it might constitute another group of potential heterodisulfide reductase associated hydrogenases (Fig. 3a). Alternatively, if Ehi did not form a complex with HdrD, it would be functionally more similar to the Ehb-type hydrogenase.

In LCB70, as in the first description of Methanomethylicia MAGs[6], a gene with similarity to lactate dehydrogenase (GlcD) was colocated with a HdrD gene[6]. Notably, both genes were highly expressed by LCB70 during methanogenic growth (Fig. 3b and Extended Data Fig. 4c), indicating their importance to its metabolism. Lactate has been observed to be metabolized by syntrophic co-cultures, in which hydrogen produced by lactate fermentation is used by hydrogen-consuming methanogens[38,39]. Alternatively, as suggested previously[6,10,16], these genes may enable lactate to be used as an electron donor to a Ehi/HdrD complex for the reduction of CoM-S-S-CoB, a property that has not been observed in any cultured Euryarchaeal methanogen. Additionally, we identified a second cluster of genes with two additional HdrD copies located adjacent to a gene containing a lactate utilization domain (LUD)[40] and a [4Fe-4S] dicluster domain (Fig. 3a; LldG-like; Extended Data Fig. 4d). Interestingly, earlier analyses of Methanomethylicia MAGs had identified GlcD-like, but not LldG-like genes. However, during methanogenic growth, LCB70 expressed these genes at low levels compared with GlcD, suggesting that they might play an alternative metabolic role (Fig. 3b). For additional discussion on the potential for lactate metabolism, see Supplementary Information. In summary, genomics and transcriptomics demonstrated growth of LCB70 by methyl-reducing hydrogenotrophic methanogenesis from methanol and hydrogen.

Ultrastructure of strain LCB70

Cultivation of LCB70 allowed us to visualize the ultrastructure of a methanogen outside the Euryarchaeota. We initially imaged a set of plunge-frozen cells of an active LCB70 culture by means of cryo-ET[41]. According to FISH, LCB70 cells were the only coccoid archaeal cells in

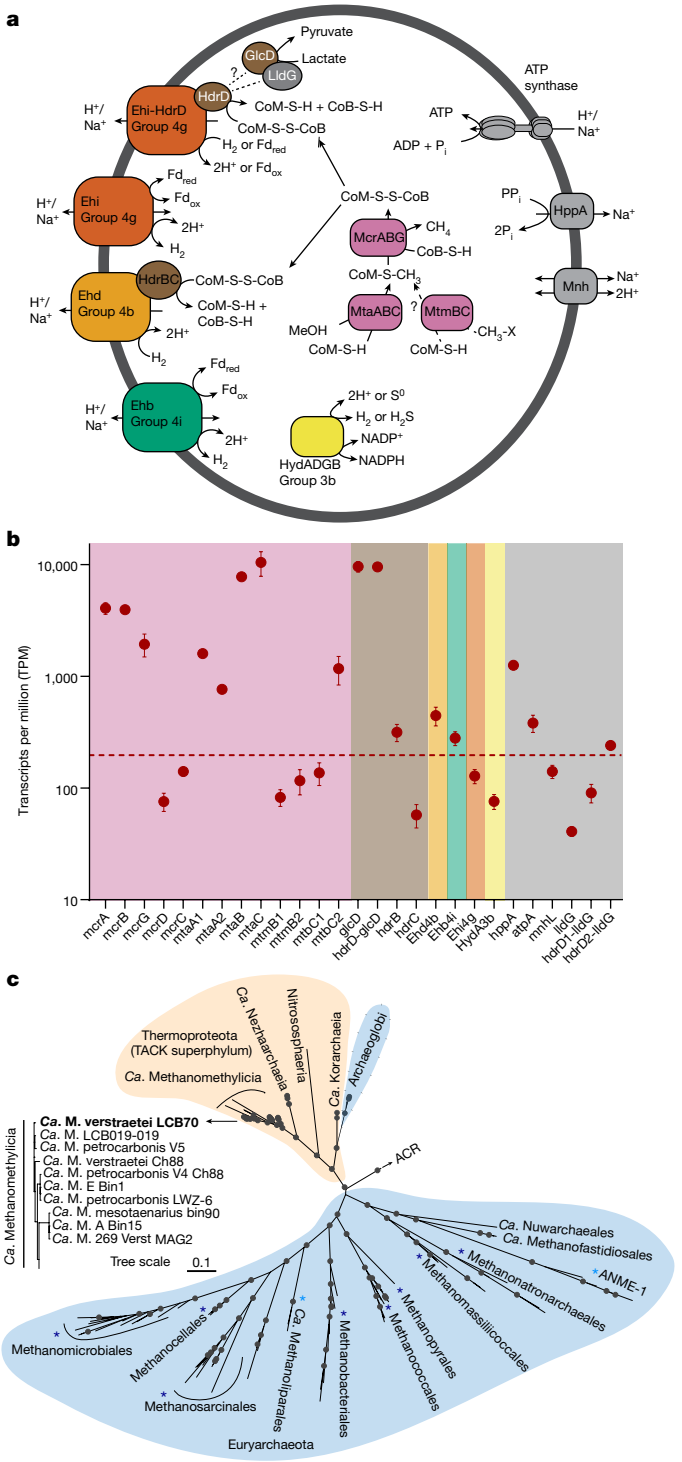

Fig. 3 | Proposed methane and hydrogen metabolism in *Ca.* M. verstraetei strain LCB70. a, Metabolic reconstruction of methyl-reducing methanogenesis and energy conservation pathways in LCB70. A list of genes used to construct this figure can be found in Supplementary Table 4. **b**, Transcriptional activity of LCB70 during growth on methanol and hydrogen with lactate. Data are mean ± s.d. ($n = 3$ biological replicates). Where not visible, the error bar is smaller than the symbol. Dashed line represents the average TPM of all genes. For transcriptomic analyses of LCB70 when grown under the addition of pyruvate or acetate, see Extended Data Fig. 4c and Supplementary Table 4. **c**, Phylogenetic tree of McrA sequences demonstrating the affiliation of LCB70 McrA within the Methanomethylicia (Thermoproteota; tan shading). Asterisks indicate lineages with isolates (dark blue) or enrichments (light blue) within the Euryarchaeota (blue shading), circles indicate bootstrap support values greater than 95. ACR, alkyl-coenzyme M reductase.

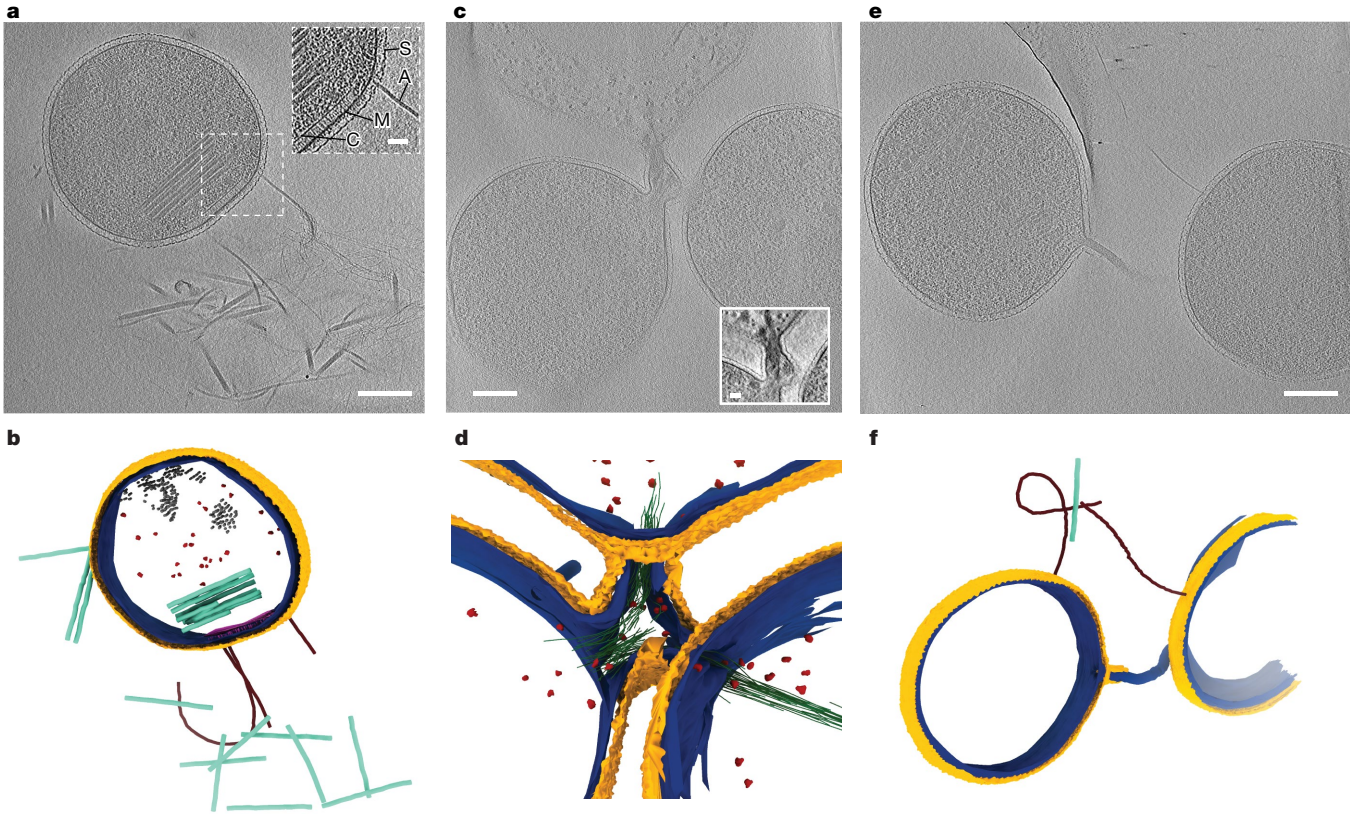

Fig. 4 | Cryoelectron tomography of LCB70 cells. a,**b**, Tomographic slice (**a**) and corresponding model (**b**) of a LCB70 cell. The S-layer (S) is shown in yellow, the cytoplasmic membrane (M) in blue, putative ribosomes in red, archaella (A) in brown, putative virus-like particles in cyan, chemoreceptor (C) arrays in purple and unidentified semi-ordered filamentous structures in grey. The latter structures were not observed in tomograms of a later culture. Inset in **a** shows a magnified view (but different Z slice) of the tomogram. **c**,**d**, Tomographic slice (**c**) and corresponding model (**d**) of a three-way cell junction (inset in **c** shows higher contrast image) with a continuous cytoplasmic membrane and S-layer that connects three cells. Putative ribosomes (red), and thin unidentified filaments (green) are located inside the cell junction. Some of these filaments are contained within the volume connecting the three cells, whereas others span from one cell to another. **e**,**f**, Tomographic slice (**e**) and corresponding model (**f**) of two LCB70 cells connected by a cell–cell bridge that is only partially covered by an S-layer. For all tomographic slices the thickness is 18.04 nm. Scale bars, 200 nm (**a**,**c**,**e**); 50 nm (insets in **a**,**c**,**e**).

the enrichment (Fig. 1c). Their unique shape, high relative abundance, and presence of an S-layer (a gene encoding an S-layer protein was highly expressed in our transcriptomic datasets; Supplementary Table 4) enabled the identification of LCB70 cells in tomograms. The LCB70 cells were surrounded by a cytoplasmic membrane and an S-layer and had an average diameter of 845 ± 163 nm (n = 55 cells; Fig. 4 and Extended Data Fig. 7). We also visualized archaella and chemoreceptor arrays in tomograms of LCB70 (Fig. 4a and Extended Data Fig. 7). Consistently, LCB70 expressed a cluster of archaella and chemotaxis genes, with the structural archaellin protein ArlB being the highest expressed within this gene cluster (Extended Data Fig. 6). This indicates that LCB70 is motile and capable of sensing and responding to environmental stimuli[42–44]. Other structures observed include putative filamentous and spindle-shaped virus-like particles, unidentified intracellular semi-ordered filamentous structures and putative storage granules (Fig. 4, Extended Data Figs. 7 and 8 and Supplementary Video 1). Confocal Raman microspectroscopy of single LCB70 cells identified by FISH (n = 18) indicated that these granules are probably glycogen. This is consistent with the expression of genes involved in glycogen synthesis and metabolism (Extended Data Fig. 7 and Supplementary Table 4).

Additional tomograms of LCB70 cells acquired from cultures grown in the presence of lactate, pyruvate or acetate, approximately a year after the first dataset had been collected, yielded consistent results for the morphology and presence of archaella, chemoreceptor arrays and storage granules across treatments (Extended Data Figs. 6c and 8). However, LCB70 cells lacked the abundant semiordered filamentous structures observed in the earlier culture, suggesting that these structures are probably not involved in the central metabolism of LCB70 (Extended Data Fig. 8).

During FISH analyses we observed LCB70 cells sometimes forming aggregates (Fig. 1c and Extended Data Fig. 9), suggesting that they might be able to form direct cell–cell interactions. Indeed, using cryo-ET, we observed cell–cell bridges between LCB70 cells with a continuous cytoplasmic membrane (n = 4) and in some cases a continuous (n = 1) or semicontinuous (n = 2) S-layer (Fig. 4 and Extended Data Fig. 10). We did not observe cell–cell bridges between LCB70 and other cell types, suggesting that either these interactions are LCB70-specific or that direct interspecies cellular connections are rare. We also visualized cell–cell bridging structures with larger compartments, which resembled vesicles (Fig. 4 and Extended Data Fig. 10). We interpret these structures to be potential intermediate forms of the same cell–cell bridges surrounded by an S-layer that connect LCB70 cells. In one tomogram, the volume of a cell–cell bridge (120–140 nm inner diameter, 160–220 nm outer diameter) shared by three cells contained both putative ribosomes and thin filaments of unknown composition (Fig. 4c,d, Extended Data Fig. 10 and Supplementary Video 2). At this point, we can only speculate about the nature of these interactions and how they form.

In bacteria, cell–cell bridges, including nanotubes, have been shown to be involved in diverse intraspecies and interspecies interactions, including the exchange of metabolites, electrons and DNA[45]. Although their function in archaea is not well understood, cell–cell bridges and other cell–cell connections have been observed in at least three

different archaeal phyla[46]. Cell–cell bridges of LCB70 cells (29–38 nm inner diameter; 71–73 nm outer diameter) most closely resemble those observed in *Haloferax volcanii* (57–162 nm outer diameter). Similar to LCB070, *H. volcanii* nanotubes are covered by a continuous S-layer and occasionally contain ribosomes and filaments that are speculated to enable cytoplasmic exchange between cells[47].

Conclusions

In summary, we demonstrate methyl-reducing hydrogenotrophic methanogenesis by *Ca*. M. verstraetei strain LCB70, a methanogen outside the Euryarchaeota, through enrichment cultivation, growth experiments, single-cell activity measurements, conversion of isotopically labelled methanol, metabolic reconstructions and transcriptomics. We also provide insight into the ultrastructure of a non-euryarchaeal methanogen, revealing structures related to motility, chemotaxis, storage granules, and cell–cell connections that may enable exchange of cytoplasmic material. Given the global distribution of these methanogens in diverse anoxic habitats, *Ca*. M. verstraetei and its close relatives[30] probably contribute to anaerobic carbon-cycling dynamics in both natural and engineered environments. Future culture-dependent studies of *Ca*. M. verstraetei will focus on the biochemistry and regulation of methanogenesis in addition to structural and functional aspects of their cell biology.

Online content

Any methods, additional references, Nature Portfolio reporting summaries, source data, extended data, supplementary information, acknowledgements, peer review information; details of author contributions and competing interests; and statements of data and code availability are available at https://doi.org/10.1038/s41586-024-07631-6.

1. Thauer, R. K., Kaster, A.-K., Seedorf, H., Buckel, W. & Hedderich, R. Methanogenic archaea: ecologically relevant differences in energy conservation. *Nat. Rev. Microbiol.* **6**, 579–591 (2008).
2. Garcia, P. S., Gribaldo, S. & Borrel, G. Diversity and evolution of methane-related pathways in archaea. *Annu. Rev. Microbiol.* **76**, 727–755 (2022).
3. Borrel, G. et al. Wide diversity of methane and short-chain alkane metabolisms in uncultured archaea. *Nat Microbiol* **4**, 603–613 (2019).
4. Wang, Y., Wegener, G., Hou, J., Wang, F. & Xiao, X. Expanding anaerobic alkane metabolism in the domain of Archaea. *Nat. Microbiol.* **4**, 595–602 (2019).
5. Evans, P. N. et al. Methane metabolism in the archaeal phylum Bathyarchaeota revealed by genome-centric metagenomics. *Science* **350**, 434–438 (2015).
6. Vanwonterghem, I. et al. Methylotrophic methanogenesis discovered in the archaeal phylum Verstraetearchaeota. *Nat. Microbiol.* **1**, 1–9 (2016).
7. Saunois, M. et al. The Global Methane Budget 2000-2017. *Earth Syst. Sci. Data* **12**, 1561–1623 (2020).
8. Conrad, R. The global methane cycle: recent advances in understanding the microbial processes involved. *Environ. Microbiol. Rep.* **1**, 285–292 (2009).
9. Thauer, R. K. Methyl (Alkyl)-Coenzyme M reductases: nickel F-430-containing enzymes involved in anaerobic methane formation and in anaerobic oxidation of methane or of short chain alkanes. *Biochemistry* **58**, 5198–5220 (2019).
10. Evans, P. N. et al. An evolving view of methane metabolism in the Archaea. *Nat. Rev. Microbiol.* **17**, 219–232 (2019).
11. Stephenson, M. & Stickland, L. H. Hydrogenase: the bacterial formation of methane by the reduction of one-carbon compounds by molecular hydrogen. *Biochem. J.* **27**, 1517–1527 (1933).
12. Rinke, C. et al. A standardized archaeal taxonomy for the Genome Taxonomy Database. *Nat. Microbiol.* **6**, 946–959 (2021).
13. Seitz, K. W. et al. Asgard archaea capable of anaerobic hydrocarbon cycling. *Nat. Commun.* **10**, 1822 (2019).
14. McKay, L. J. et al. Co-occurring genomic capacity for anaerobic methane metabolism and dissimilatory sulfite reduction discovered in the *Korarchaeota*. *Nat. Microbiol.* **4**, 614–622 (2019).
15. McKay, L. J., Hatzenpichler, R., Inskeep, W. P. & Fields, M. W. Occurrence and expression of novel methyl-coenzyme M reductase gene (*mcrA*) variants in hot spring sediments. *Sci. Rep.* **7**, 7252 (2017).
16. Hua, Z.-S. et al. Insights into the ecological roles and evolution of methyl-coenzyme M reductase-containing hot spring Archaea. *Nat. Commun.* **10**, 4574 (2019).
17. Lynes, M. M. et al. Diversity and function of methyl-coenzyme M reductase-encoding archaea in Yellowstone hot springs revealed by metagenomics and mesocosm experiments. *ISME Commun.* **3**, 22 (2023).
18. Buessecker, S. et al. Mcr-dependent methanogenesis in Archaeoglobaceae enriched from a terrestrial hot spring. *ISME J.* **17**, 1649–1659 (2023).
19. Wang, J. et al. Evidence for nontraditional mcr-containing archaea contributing to biological methanogenesis in geothermal springs. *Sci. Adv.* **9**, eadg6004 (2023).
20. Lynes, M. M., Jay, Z. J., Kohtz, A. J. & Hatzenpichler, R. Methylotrophic methanogenesis in the Archaeoglobi revealed by cultivation of Ca. Methanoglobus hypatiae from a Yellowstone hot spring. *ISME J.* **18**, wrae026 (2024).
21. Liu, Y.-F. et al. Long-term cultivation and meta-omics reveal methylotrophic methanogenesis in hydrocarbon-impacted habitats. *Engineering* **24**, 264–275 (2023).
22. Oren, A., Garrity, G. M., Parker, C. T., Chuvochina, M. & Trujillo, M. E. Lists of names of prokaryotic Candidatus taxa. *Int. J. Syst. Evol. Microbiol.* **70**, 3956–4042 (2020).
23. Zeikus, J., Ben-Bassat, A. & Hegge, P. Microbiology of methanogenesis in thermal, volcanic environments. *J. Bacteriol.* **143**, 432–440 (1980).
24. McKay, L. J., Klingelsmith, K. B., Deutschbauer, A. M., Inskeep, W. P. & Fields, M. W. Draft genome sequence of Methanothermobacter thermautotrophicus WHS, a thermophilic hydrogenotrophic methanogen from Washburn Hot Springs in Yellowstone National Park, USA. *Microbiol. Resour. Announc.* **10**, e01157–01120 (2021).
25. Cheng, L., Dai, L., Li, X., Zhang, H. & Lu, Y. Isolation and characterization of Methanothermobacter crinale sp. nov., a novel hydrogenotrophic methanogen from the Shengli oil field. *Appl. Environ. Microbiol.* **77**, 5212–5219 (2011).
26. Balk, M., Weijma, J. & Stams, A. J. Thermotoga lettingae sp. nov., a novel thermophilic, methanol-degrading bacterium isolated from a thermophilic anaerobic reactor. *Int. J. Syst. Evol. Microbiol.* **52**, 1361–1368 (2002).
27. Paulo, P. et al. Pathways of methanol conversion in a thermophilic anaerobic (55 C) sludge consortium. *Appl. Microbiol. Biotechnol.* **63**, 307–314 (2003).
28. Hatzenpichler, R., Krukenberg, V., Spietz, R. L. & Jay, Z. J. Next-generation physiology approaches to study microbiome function at single cell level. *Nat. Rev. Microbiol.*, **18**, 241–256 (2020).
29. Hatzenpichler, R. et al. Visualizing in situ translational activity for identifying and sorting slow-growing archaeal– bacterial consortia. *Proc. Natl Acad. Sci. USA* **113**, E4069–E4078 (2016).
30. Wu, K. et al. Isolation of a methyl-reducing methanogen outside the Euryarchaeota. *Nature* https://doi.org/10.1038/s41586-024-07728-y (2024).
31. Kohtz, A. J., Jay, Z. J., Lynes, M. M., Krukenberg, V. & Hatzenpichler, R. Culexarchaeia, a novel archaeal class of anaerobic generalists inhabiting geothermal environments. *ISME Commun.* **2**, 1–13 (2022).
32. Major, T. A., Liu, Y. & Whitman, W. B. Characterization of energy-conserving hydrogenase B in Methanococcus maripaludis. *J. Bacteriol.* **192**, 4022–4030 (2010).
33. Ma, K., Schicho, R. N., Kelly, R. M. & Adams, M. Hydrogenase of the hyperthermophile Pyrococcus furiosus is an elemental sulfur reductase or sulfhydrogenase: evidence for a sulfur-reducing hydrogenase ancestor. *Proc. Natl Acad. Sci. USA* **90**, 5341–5344 (1993).
34. Lang, K. et al. New mode of energy metabolism in the seventh order of methanogens as revealed by comparative genome analysis of "Candidatus Methanoplasma termitum". *Appl. Environ. Microbiol.* **81**, 1338–1352 (2015).
35. Loh, H. Q., Hervé, V. & Brune, A. Metabolic potential for reductive acetogenesis and a novel energy-converting [NiFe] hydrogenase in Bathyarchaeia from termite guts–A genome-centric analysis. *Front. Microbiol.* **11**, 635786 (2021).
36. Kröninger, L., Berger, S., Welte, C. & Deppenmeier, U. Evidence for the involvement of two heterodisulfide reductases in the energy-conserving system of Methanomassiliicoccus luminyensis. *FEBS J.* **283**, 472–483 (2016).
37. Kröninger, L. et al. Energy conservation in the gut microbe Methanomassiliicoccus luminyensis is based on membrane-bound ferredoxin oxidation coupled to heterodisulfide reduction. *FEBS J.* **286**, 3831–3843 (2019).
38. Bryant, M., Campbell, L. L., Reddy, C. & Crabill, M. Growth of Desulfovibrio in lactate or ethanol media low in sulfate in association with H2-utilizing methanogenic bacteria. *Appl. Environ. Microbiol.* **33**, 1162–1169 (1977).
39. McInerney, M. J. & Bryant, M. P. Anaerobic degradation of lactate by syntrophic associations of Methanosarcina barkeri and Desulfovibrio species and effect of H2 on acetate degradation. *Appl. Environ. Microbiol.* **41**, 346–354 (1981).
40. Hwang, W. C. et al. LUD, a new protein domain associated with lactate utilization. *BMC Bioinf.* **14**, 1–9 (2013).
41. Young, L. N. & Villa, E. Bringing Structure to Cell Biology with Cryo-Electron Tomography. *Annu. Rev. Biophys.* **52**, 573–595 (2023).
42. Briegel, A. et al. Structural conservation of chemotaxis machinery across A rchaea and B acteria. *Environ. Microbiol. Rep.* **7**, 414–419 (2015).
43. Albers, S.-V. & Jarrell, K. F. The archaellum: an update on the unique archaeal motility structure. *Trends Microbiol.* **26**, 351–362 (2018).
44. Quax, T. E., Albers, S.-V. & Pfeiffer, F. Taxis in archaea. *Emerg. Top. Life Sci.* **2**, 535–546 (2018).
45. Baidya, A. K., Bhattacharya, S., Dubey, G. P., Mamou, G. & Ben-Yehuda, S. Bacterial nanotubes: a conduit for intercellular molecular trade. *Curr. Opin. Microbiol.* **42**, 1–6 (2018).
46. Liu, J. et al. Extracellular membrane vesicles and nanotubes in Archaea. *microLife* **2**, uqab007 (2021).
47. Sivabalasarma, S. et al. Analysis of cell–cell bridges in Haloferax volcanii using electron cryo-tomography reveal a continuous cytoplasm and S-layer. *Front. Microbiol.* **11**, 612239 (2021).

Methods

Chemicals

Unless otherwise specified, all chemicals were obtained from Sigma.

Source of inoculum and cultivation

Sediments from hot spring LCB070 (44° 34′ 01.8″ N, 110° 48′ 20.2″ W) located in the LCB thermal complex of YNP, WY, USA were obtained in October 2019. A mixture of surface sediments (approximately 1 cm deep) and water (62 °C, pH 8.2) were collected into a sterile glass bottle that was sealed with a thick butyl-rubber stopper without headspace. After transport to the lab, sediments were stored at room temperature. Enrichment cultures were established using anoxic medium containing a base of (per litre): KH_2PO_4, 0.5 g; $MgSO_4 \cdot 7H_2O$, 0.4 g; NaCl, 0.5 g; NH_4Cl, 0.4 g; $CaCl_2 \cdot 2H_2O$, 0.05 g; 2-N-morpholino-ethanesulfonic acid (MES), 2.17 g; yeast extract, 0.1 g; and 0.002% (w/v) $(NH_4)_2Fe(SO_4)_2 \cdot 6H_2O$, 5 mM $NaHCO_3$, 1 ml trace element solution SL-10, 1 ml Selenite-Tungstate solution, 1 ml CCM vitamins[48], 0.0005% (w/v) resazurin, 10 mg of coenzyme-M, 2 mg sodium dithionite, 1 mM dithiothreitol and 1 mM $Na_2S \cdot 9H_2O$. The pH was adjusted to 6.5. Sediment slurry was added (10% v/v) and vials were sealed with thick butyl-rubber stoppers and aluminium crimps in an anoxic glove box (Coy). The headspace of the enrichments was sparged with N_2:CO_2 (90:10) for 5 min and set to 200 kPa. Methanol and hydrogen were added to a final concentration of 10 mM and 50%, respectively. The cultures were incubated at 64 °C in the dark without shaking. Batch cultures were maintained by transfer of 10% v/v inoculum into fresh medium. A sediment-free culture was obtained after three transfers, after which the culture was maintained on increased methanol concentrations of 40–50 mM and the addition of 10 mM sodium L-lactate as an additional carbon source. Replicate cultures for comparing methane production with or without hydrogen and methanol were performed in duplicate in 30 ml incubation volumes in a 60 ml serum bottle.

Fluorescence in situ hybridization and biovolume calculation

Subsamples were chemically fixed with paraformaldehyde (PFA, 2% final concentration) for 1 h at room temperature, then washed and stored in PBS buffer at 4 °C. An oligonucleotide probe targeting most Methanomethyliciaceae 16S rRNA sequence contained in the Silva[49] database (v.132) was designed using the probe design tool in ARB[50] (Msur657, 5′-CCCTCAACCTCTCCCGCC-3′). According to TestProbe[49] using the Silva138 database, this probe detects 71% of 16S rRNA sequences within the family Methanomethyliaceae, and only binds two non-target sequences outside that group. Both sequences are found in the Geoarchaeales, which are absent from our enrichment culture. DOPE-FISH was performed as previously described[51] using the Msur657 probe doubly labelled with FAM (obtained from IDT-DNA). To track *Ca*. M. verstraetei LCB70 and other archaeal cells, a general archaea-targeted probe Arch915[52], double-labelled with Alexa Fluor 647, was used in combination with the FAM-labelled Msur657 probe and the DNA-stain 4′,6-diamidino-2-phenylindole (DAPI). All hybridization reactions were carried out at a formamide concentration of 35% (Supplementary Table 6). Negative controls used double-labelled NONEUB338[53] and were performed in parallel at a formamide concentration of 35%.

Because the enrichment contained cell aggregates that could not be disassociated (for example, by sonication or detergent addition) quantitative FISH on a per-cell basis was not possible. Instead, biovolume fractions of LCB70 (cells that bound Msur657 and Arch915) and other archaea (cells that bound to Arch915) in the culture was performed as previously described[54]. In brief, PFA-fixed biomass was applied to a slide and DOPE-FISH was performed with the Msur657 and Arch915 as described above, followed by counterstaining with DAPI and embedding in Citifluor. Cells were imaged with a Leica DM4B epifluorescence microscope. Images were segmented and biovolumes calculated with the daime software package[55].

DNA extraction and metagenome sequencing

Hot spring sediment from site LCB070 was collected in October 2019 using a sterile metal cup and was immediately frozen in a dry ice–ethanol bath. DNA was extracted from 10 ml of sediment following the protocol described previously[56]. Truseq libraries were prepared and sequenced at the DOE Joint Genome Institute (JGI) on the Illumina NovaSeq S4 platform following a 2 × 150 bp indexed run recipe.

Under anoxic conditions, 15 ml of the first transfer of the LCB70 culture was collected and centrifuged at 16,000*g* for 5 min to pellet cells. The supernatant was then removed and the pellet stored at −80 °C. Genomic DNA was extracted from the cell pellet using the protocol described previously[56], with the following modifications. The proteinase K step was extended to 1 h and the precipitation was performed in the presence of 0.7× volumes isopropanol and 0.1× volume of 3 M sodium acetate. Crude extracts were purified using a Zymo clean and concentrator kit (DCC-10, Zymo Research) according to the manufacturer's instructions. Purified genomic DNA was shipped to the Michigan State University genomics core for library preparation and sequencing. A metagenomic library was constructed with the TruSeq Nano DNA kit according to the manufacturer's recommendations. The library was sequenced on an Illumina NovaSeq 6000 platform using the NovaSeq XP reagent kits, SP flow cell, and followed a 2 × 150 bp indexed run recipe.

Nanopore long-read sequencing was performed using a MinION platform and a R9.4.1 flow cell (Oxford Nanopore Technologies). Library preparation was performed using the rapid kit (SQK-RBK004) according to the manufacturer's instructions. Flow cells were run for 72 h, resulting in 1.3 Gbp of total sequence data. Base-calling was performed with Guppy (v5.0.16+b9fcd7b) using model dna_r9.4.1_450bps_hac and parameters, --trim_barcodes, --detect_mid_strand_adapter and --detect_mid_strand_barcodes.

Metagenome assembly, binning, and quality assessment

For the sediment metagenome from site LCB070, raw metagenomic reads were processed according to JGI's standard workflow, and quality-controlled reads were assembled using SPAdes (v.3.14.1)[57] with options -m 2000 -k 33,55,77,99,127 and -meta. For the enrichment culture metagenome, Illumina reads were evaluated with FastQC (v.0.11.5) to determine best parameters before trimming (quality, linker and adapter). Artefact and common contaminant removal was done with rqcfilter2 (maxns=3, maq=3, minlen=51) followed by error correction with bbcms (mincount=2, hcf=0.6) from the BBTools suite (v.38.94)[58]. Resulting reads were assembled with SPAdes (v.3.15.3; -k 33,55,77,99,111 -meta –only-assembler) and coverage was determined by mapping the cleaned and corrected reads to the assembled sequences with bbmap (ambiguous=random). Assembled sequences greater than or equal to 2,000 bp in length were binned with four programs: Maxbin (v.2.2.7)[59], Concoct (v.1.0.0)[60], Metabat (v.2.12.1; with and without coverage)[61] and Autometa (v.1; bacterial and archaeal modes, including the machine learning step)[62] followed by bin refinement with DAS_Tool (v.1.1.2)[63], as previously described[31]. CheckM (v.1.1.3)[64] was used to assess MAG completeness and redundancy.

Assembly of the circular genome of LCB70

A long-read assembly was created using nanopore reads with metaFlye (v.2.8.2), specifying three polishing iterations[65]. This step produced a circular assembly of the LCB70 genome. Long-read polishing was done with Medaka (v.1.5.0), consisting of mini_align, medaka_consensus, the model 941_min_hac_g507 and the medaka stitch commands. Following this, Polypolish[66] was used to polish the assembly three times with the Illumina reads. Finally, three additional rounds of polishing

using the Illumina reads were carried out with Polca[67], producing a final polished assembly.

Amplicon sequencing and analysis

A 1 ml aliquot of culture was pelleted by centrifugation (16,000*g*; 5 min) and DNA from the cell pellet was extracted using the FastDNA Spin Kit for Soil (MP Biomedicals) following the manufacturer's guidelines. Archaeal and bacterial 16S rRNA genes were amplified with the Earth Microbiome Project primer set 515 F and 806R[68,69], amplicon libraries were prepared as described previously[70], and sequencing was performed at the Molecular Research Core Facility at Idaho State University (Pocatello, ID) using an Illumina MiSeq platform with 2 × 250 bp paired end read chemistry. Reads were processed as described previously[70] with QIIME 2 (v.2020.2)[71]. In brief, barcode sequences were removed with cutadapt and then reads were truncated (209 forward, 215 reverse). Reads were denoised, merged and chimera-checked with DADA2[72] using default settings. Taxonomic assignment of amplicon sequence variants was done using the sklearn method and the Silva SSU database[49] release 132.

Phylogenetic analyses

The 16S rRNA sequences encoded in publicly available Methanomethylicia MAGs were aligned and masked against reference archaeal 16S rRNA sequences using SSU-ALIGN (v.0.1.1)[73], which produced a final alignment of 1,376 positions. Maximum likelihood analysis was performed using FastTree (v.2.1.10) and default parameters.

A set of 33 single-copy marker proteins (Supplementary Table 5) were collected from Methanomethylicia MAGs and reference archaeal genomes. These markers were aligned with MUSCLE[74], trimmed with trimAL[75] using a 50% gap threshold, and concatenated to produce a final alignment of 7,118 positions. IQtree2 was used to reconstruct a maximum likelihood phylogenetic tree and ModelFinder[76] was used to select the best fit model with the additional option –madd LG + C60,LG + C60 + F + G,LG + C60 + F + R. The best fit LG + F + R10 model was selected according to Bayesian inference criterion and branch support was evaluated with 1,000 ultrafast bootstraps and 1,000 iterations of the SH-like approximate-likelihood ratio test[77].

The McrA sequence of LCB70 was aligned against a set of publicly available reference sequences using MAFFT-linsi[78], trimmed with trimAL using a 50% gap threshold. A maximum likelihood phylogenetic tree was reconstructed using IQtree2, using the LG + C60 + F + G model and 1,000 ultrafast bootstraps.

Sequences of catalytic subunits of group 4 [NiFe]-hydrogenases encoded by LCB70 were aligned against the HydDB reference sequences and reference FpoD/NuoD subunits. Additional Ehi sequences were collected through Blastp searches of the NCBI nr and IMG databases using the strain LCB70 sequence as a query. References were aligned with MAFFT-linsi and trimmed with trimAL using a 50% gap threshold, producing a final alignment of 365 residues. Maximum likelihood phylogenetic trees were constructed with IQtree2 with the model LG + C60 + R + F and 1,000 ultrafast bootstraps.

Annotation and reconstruction of metabolic potential

MAGs were annotated using Prokka (v.1.14.6)[79] with both default and custom/in-house annotation databases. Refinement and confirmation of the initial annotation was done by submission of protein sequences to the NCBI conserved domain database[80] and HHpred[81] using default settings. Furthermore, the strain LCB70 genome was uploaded to the IMG/M database for annotation[82]. The catalytic subunits of [NiFe] hydrogenases were submitted to HydDB[83] for classification and further confirmed through phylogenetic analysis (above).

RNA extraction, sequencing, and analysis

Enrichment cultures of LCB70 were grown in triplicate in 30 ml of media with 100 mM methanol and hydrogen (50%) and supplemented with 10 mM of either lactate, pyruvate or acetate. During the exponential phase of methane production, culture bottles were rapidly cooled from 64 °C by putting them in an ice bath that was placed at −20 °C for 15 min; vials were subsequently kept on ice during the procedure. Cells were concentrated by centrifugation at 12,000*g* for 10 min and the cell pellet was resuspended in 800 µl of Zymo DNA/RNA Shield and stored at 4 °C overnight. The following day, cells were mixed 1:1 with Zymo RNA lysis buffer and added to Zymo BashingBead lysis tubes (Zymo Research) and vortexed at maximum speed for 10 min. The tubes were centrifuged at 14,000*g* for 15 min and RNA was purified from the supernatant with a Zymo Quick-RNA miniprep kit according to the manufacturer's instructions and including the DNAse I step. Extracted RNA was sent to SeqCenter (Pittsburgh, PA), which provided an additional DNAse I treatment (Invitrogen), library preparation and sequencing. Libraries were prepared with Illumina's Stranded Total RNA Prep Ligation with Ribo-Zero Plus kit and 10 bp unique dual indices. Sequencing of the libraries was performed on a NovaSeq X Plus platform producing 2 × 150 bp reads. bcl-convert (v.4.1.5) was used for demultiplexing, quality control and adapter trimming. Reads were then processed with rqcfilter2 (rna=t, trimrnaadapter=t, qtrim=rl, trimq=10, maq=20, maxn=0, minlen=50, mlf=0.33, removeribo=f) and mapped to the genes of all MAGs obtained from the culture using salmon (v.1.10.2; --validateMappings --seqBias)[84]. Reads mapping to rRNA genes were excluded before normalization. Reads mapping to each gene were normalized to gene length and expressed as transcripts per kilobase million (TPM).

Chemical analyses of methane and methanol

During cultivation, 250 µl subsamples of the headspace were taken with a gas-tight syringe (Hamilton) and injected into 10 ml autosampler vials that had been sealed with grey chlorobutyl septa. Samples were taken from the autosampler vials and injected into a Shimadzu 2020-GC gas chromatograph equipped with a GS-CarbonPLOT column (30 m × 0.32 mm; 1.5 µm film thickness; Agilent) and a Rt-Q-BOND column (30 m × 0.32 mm; 1.5 µm film thickness; Restek) using Helium as a carrier gas. The injector, column and flame ionization detector (FID) were maintained at 200 °C, 50 °C and 240 °C, respectively. Methane concentrations were calculated based on injection of a standard curve. For methanol quantification, 500 µl liquid subsamples were taken with a needle and syringe and placed immediately on ice. The liquid was cleared by centrifugation (16,000*g*; 5 min; 4 °C). Then, 400 µl of supernatant was placed in a sealed, gas-tight 10 ml vial and stored at −20 °C. For analysis, the liquid was heated to 80 °C for 5 min and then 500 µl of headspace was injected into the Shimadzu 2020-GC gas chromatograph. Methanol concentrations were calculated based on injection of a standard curve. All injections on the Shimadzu 2020-GC were performed with a robotic autosampler (AOC-6000).

BONCAT–FISH and inhibition experiments

Experiments were carried out in 30 ml culture volumes in 60 ml serum bottles. A control bottle contained 10 mM BES inhibitor at the start of the experiment. After 10 days of growth one set of replicate cultures was spiked with 10 mM BES and the cultures were incubated for 48 h, after which 100 µM of the amino acid analogue HPG was added to all cultures, except a no HPG control bottle. After HPG addition, the cultures were incubated for 24 h, and subsamples were fixed in PFA for BONCAT–FISH analyses. The azide-alkyne click chemistry reaction was performed as previously described[29] and used azide-labelled TexasRed (Click Chemistry Tools). Following the click chemistry reaction, DOPE-FISH was performed as described above with a 2xFAM labelled Msur657 probe.

Stable isotope tracing

To track the conversion of ^{13}C-methanol to ^{13}C-methane (^{13}C-CH_4), active cultures were incubated in the presence of ^{12}C-methanol or ^{13}C-methanol under a 90% N_2, 10% CO_2 headspace. During the incubation, headspace

samples were injected into a Shimadzu QP2020 NX GCMS equipped with a GS-CarbonPLOT column (30 m × 0.35 mm; 1.5 µm film thickness; Agilent) using the method previously described[85] and Helium as a carrier gas. The collection was run in Selected Ion Monitoring mode and peak areas corresponding to m/z of 16 for $^{12}CH_4$, 17 for $^{13}CH_4$, 44 for $^{12}CO_2$ and 45 for $^{13}CO_2$ were used for quantification. All injections on the Shimadzu QP2020 NX GCMS were performed with a robotic autosampler (AOC-6000).

Habitat distribution

The 16S rRNA gene sequence for strain LCB70 was submitted to the IMNGS webserver[86] to search the NCBI Sequence Read Archive (SRA) for sequences with a sequence similarity cutoff of 97% and a minimum size of 200 bp. Metadata on the sample collection source was collected from each SRA sample that had sequence hits.

Plunge freezing for cryo-ET

Enrichment cultures containing LCB70 grown at 64 °C with different nutrition sources (lactate, acetate, pyruvate) or treated with BES (with lactate) were plunge frozen. For the initial data collection, the following steps were performed inside an anoxic glove box: 500 µl of the enrichment culture grown with lactate were centrifuged at 16,000*g* for 10 min at 20 °C and the resulting pellet was resuspended in 100 µl of the supernatant. All other sample preparations were performed without the concentration step to keep the samples at 64 °C and to avoid potential artefacts. All samples were mixed with Protein A-conjugated 10 nm colloidal gold before plunge freezing. Afterwards, the culture was removed from the glove box and, within a few seconds during which the culture was exposed to laboratory air, 3.5 µl of the enrichment culture were then applied to glow-discharged copper EM grids (R2/1, Quantifoil), automatically blotted for 4, 8 or 10 s and plunged into liquid ethane using a Vitrobot Mark IV (Thermo Fisher Scientific)[87]. The plunge-frozen grids were clipped into autogrids, stored in liquid nitrogen and shipped to ETH Zurich in a liquid nitrogen cooled dry shipper.

Cryo-ET

The cryo-ET datasets were collected on a Titan Krios G4 EM (ThermoFisher) operating at 300 kV and equipped with BioContinuum imaging energy filter (slit width 20 eV) and a K3 Summit camera (Gatan). The tilt series were collected at a magnification of 19,500 (effective pixel size 4.51 Å) with a defocus of −8 µm using a bidirectional scheme from −60° to +60° in 2° incremental steps using SerialEM[88]. The total dose of a tilt series was 165 to 180 $e^-/Å^2$.

Tomogram reconstruction and segmentation

Strain LCB70 cells were identified by their morphology (determined by FISH), their high relative abundance in the culture, and their S-layer. Three-dimensional (3D) tomograms were generated using gold fiducial alignment and weighted-back projection reconstruction in the IMOD software package[89,90]. To increase contrast, the tomogram shown in Fig. 4c (inset) was filtered using tom-deconv deconvolution filter[91]. The 3D segmentations of tomograms and videos were generated using IMOD or UCSF Chimera X[92]. The cellular features were segmented manually.

Confocal Raman microspectroscopy

Correlative FISH-Raman microscopy was performed as previously described[93]. Succinctly, single LCB70 cells were identified on stainless-steel slides by dual hybridization with the Msur657 and Arch915 probes as described above. Single-cell Raman spectra were acquired using the 532 nm laser on a LabRAM HR Evolution Confocal Raman microscope (Horiba Jobin-Yvon) equipped with 300 grooves per millimetre diffraction grating and a ×100 dry objective. For each cell (n = 18), four acquisitions of 10 s each were collected from 400 to 3,200 cm^{-1} at a laser power of 4.5 mW. Spectra were processed using the LabSpec software package (v.6.5.1.24, Horiba), baselined, normalized to the maximum intensity within the 2,800–3,100 cm^{-1} region. Raman spectra were analysed for the presence of indicator peaks of glycogen (478–484, 840–860 and 930 cm^{-1}), polyhydroxyalkanoates (432, 840 and 1,726 cm^{-1}), and polyphosphate (690 and 1,170 cm^{-1})[94,95].

Reporting summary

Further information on research design is available in the Nature Portfolio Reporting Summary linked to this article.

Data availability

The LCB70 enrichment culture metagenomic, metatranscriptomic, and amplicon data are deposited under NCBI BioProject ID PRJNA916083. The LCB070 hot spring metagenome is publicly available on the IMG database under the taxon ID 3300043544 and the strain LCB70 genome under taxon ID 8012933652. Cryo-tomograms are deposited at EMDB/EMPIAR under accession numbers EMD-50298 to EMD-50305, EMD-50308 to EMD-50313 and EMD-50315. Raman spectra are available in the MicrobioRaman database (https://www.ebi.ac.uk/biostudies/MicrobioRaman/studies) with accession number S-MBRS7. Source data are provided with this paper.

48. Brandis, A. & Thauer, R. K. Growth of Desulfovibrio species on hydrogen and sulphate as sole energy source. *Microbiology* **126**, 249–252 (1981).
49. Quast, C. et al. The SILVA ribosomal RNA gene database project: improved data processing and web-based tools. *Nucleic Acids Res.* **41**, D590–D596 (2012).
50. Ludwig, W. et al. ARB: a software environment for sequence data. *Nucleic Acids Res.* **32**, 1363–1371 (2004).
51. Stoecker, K., Dorninger, C., Daims, H. & Wagner, M. Double labeling of oligonucleotide probes for fluorescence in situ hybridization (DOPE-FISH) improves signal intensity and increases rRNA accessibility. *Appl. Environ. Microbiol.* **76**, 922–926 (2010).
52. Stahl, D. A. in *Nucleic Acid Techniques in Bacterial Systematics* (eds Stackebrandt, E. & Goodfellow, M.) 205–248 (Wiley, 1991).
53. Wallner, G., Amann, R. & Beisker, W. Optimizing fluorescent in situ hybridization with rRNA-targeted oligonucleotide probes for flow cytometric identification of microorganisms. *Cytom.: J. Int. Soc. Anal. Cytol.* **14**, 136–143 (1993).
54. Daims, H. Use of fluorescence in situ hybridization and the daime image analysis program for the cultivation-independent quantification of microorganisms in environmental and medical samples. *Cold Spring Harb. Protoc.* **2009**, pdb. prot5253 (2009).
55. Daims, H., Lücker, S. & Wagner, M. Daime, a novel image analysis program for microbial ecology and biofilm research. *Environ. Microbiol.* **8**, 200–213 (2006).
56. Zhou, J., Bruns, M. A. & Tiedje, J. M. DNA recovery from soils of diverse composition. *Appl. Environ. Microbiol.* **62**, 316–322 (1996).
57. Nurk, S., Meleshko, D., Korobeynikov, A. & Pevzner, P. A. metaSPAdes: a new versatile metagenomic assembler. *Genome research* **27**, 824–834 (2017).
58. Bushnell, B. *BBMap: a fast, accurate, splice-aware aligner* (Lawrence Berkeley National Lab., 2014).
59. Wu, Y.-W., Tang, Y.-H., Tringe, S. G., Simmons, B. A. & Singer, S. W. MaxBin: an automated binning method to recover individual genomes from metagenomes using an expectation-maximization algorithm. *Microbiome* **2**, 1–18 (2014).
60. Alneberg, J. et al. Binning metagenomic contigs by coverage and composition. *Nat. Methods* **11**, 1144–1146 (2014).
61. Kang, D. D. et al. MetaBAT 2: an adaptive binning algorithm for robust and efficient genome reconstruction from metagenome assemblies. *PeerJ* **7**, e7359 (2019).
62. Miller, I. J. et al. Autometa: automated extraction of microbial genomes from individual shotgun metagenomes. *Nucleic Acids Res.* **47**, e57–e57 (2019).
63. Sieber, C. M. et al. Recovery of genomes from metagenomes via a dereplication, aggregation and scoring strategy. *Nat. Microbiol.* **3**, 836–843 (2018).
64. Parks, D. H., Imelfort, M., Skennerton, C. T., Hugenholtz, P. & Tyson, G. W. CheckM: assessing the quality of microbial genomes recovered from isolates, single cells, and metagenomes. *Genome Res.* **25**, 1043–1055 (2015).
65. Kolmogorov, M. et al. metaFlye: scalable long-read metagenome assembly using repeat graphs. *Nat. Methods* **17**, 1103–1110 (2020).
66. Wick, R. R. & Holt, K. E. Polypolish: short-read polishing of long-read bacterial genome assemblies. *PLoS Comput. Biol.* **18**, e1009802 (2022).
67. Zimin, A. V. & Salzberg, S. L. The genome polishing tool POLCA makes fast and accurate corrections in genome assemblies. *PLoS Comput. Biol.* **16**, e1007981 (2020).
68. Apprill, A., McNally, S., Parsons, R. & Weber, L. Minor revision to V4 region SSU rRNA 806 R gene primer greatly increases detection of SAR11 bacterioplankton. *Aquat. Microb. Ecol.* **75**, 129–137 (2015).
69. Parada, A. E., Needham, D. M. & Fuhrman, J. A. Every base matters: assessing small subunit rRNA primers for marine microbiomes with mock communities, time series and global field samples. *Environ. Microbiol.* **18**, 1403–1414 (2016).
70. Reichart, N. J. et al. Activity-based cell sorting reveals responses of uncultured archaea and bacteria to substrate amendment. *ISME J.* **14**, 2851–2861 (2020).
71. Bolyen, E. et al. Reproducible, interactive, scalable and extensible microbiome data science using QIIME 2. *Nat. Biotechnol.* **37**, 852–857 (2019).

72. Callahan, B. J. et al. DADA2: high-resolution sample inference from Illumina amplicon data. *Nat. Methods* **13**, 581–583 (2016).
73. Nawrocki, E. P., Kolbe, D. L. & Eddy, S. R. Infernal 1.0: inference of RNA alignments. *Bioinformatics* **25**, 1335–1337 (2009).
74. Edgar, R. C. MUSCLE: multiple sequence alignment with high accuracy and high throughput. *Nucleic Acids Res.* **32**, 1792–1797 (2004).
75. Capella-Gutiérrez, S., Silla-Martínez, J. M. & Gabaldón, T. trimAl: a tool for automated alignment trimming in large-scale phylogenetic analyses. *Bioinformatics* **25**, 1972–1973 (2009).
76. Kalyaanamoorthy, S., Minh, B. Q., Wong, T. K., Von Haeseler, A. & Jermiin, L. S. ModelFinder: fast model selection for accurate phylogenetic estimates. *Nat. Methods* **14**, 587–589 (2017).
77. Guindon, S. et al. New algorithms and methods to estimate maximum-likelihood phylogenies: assessing the performance of PhyML 3.0. *Syst. Biol.* **59**, 307–321 (2010).
78. Katoh, K. & Standley, D. M. MAFFT multiple sequence alignment software version 7: improvements in performance and usability. *Mol. Biol. Evol.* **30**, 772–780 (2013).
79. Seemann, T. Prokka: rapid prokaryotic genome annotation. *Bioinformatics* **30**, 2068–2069 (2014).
80. Lu, S. et al. CDD/SPARCLE: the conserved domain database in 2020. *Nucleic Acids Res.* **48**, D265–D268 (2020).
81. Zimmermann, L. et al. A completely reimplemented MPI bioinformatics toolkit with a new HHpred server at its core. *J. Mol. Biol.* **430**, 2237–2243 (2018).
82. Chen, I.-M. A. et al. IMG/M v. 5.0: an integrated data management and comparative analysis system for microbial genomes and microbiomes. *Nucleic Acids Res.* **47**, D666–D677 (2019).
83. Søndergaard, D., Pedersen, C. N. & Greening, C. HydDB: a web tool for hydrogenase classification and analysis. *Sci. Rep.* **6**, 1–8 (2016).
84. Patro, R., Duggal, G., Love, M. I., Irizarry, R. A. & Kingsford, C. Salmon provides fast and bias-aware quantification of transcript expression. *Nat. Methods* **14**, 417–419 (2017).
85. Ai, G., Zhu, J., Dong, X. & Sun, T. Simultaneous characterization of methane and carbon dioxide produced by cultured methanogens using gas chromatography/isotope ratio mass spectrometry and gas chromatography/mass spectrometry. *Rapid Commun. Mass Spectrom.* **27**, 1935–1944 (2013).
86. Lagkouvardos, I. et al. IMNGS: a comprehensive open resource of processed 16S rRNA microbial profiles for ecology and diversity studies. *Sci. Rep.* **6**, 1–9 (2016).
87. Iancu, C. V. et al. Electron cryotomography sample preparation using the Vitrobot. *Nat. Protoc.* **1**, 2813–2819 (2006).
88. Mastronarde, D. N. Automated electron microscope tomography using robust prediction of specimen movements. *J. Struct. Biol.* **152**, 36–51 (2005).
89. Kremer, J. R., Mastronarde, D. N. & McIntosh, J. R. Computer visualization of three-dimensional image data using IMOD. *J. Struct. Biol.* **116**, 71–76 (1996).
90. Mastronarde, D. Correction for non-perpendicularity of beam and tilt axis in tomographic reconstructions with the IMOD package. *J. Microsc.* **230**, 212–217 (2008).
91. Tegunov, D. & Cramer, P. Real-time cryo-electron microscopy data preprocessing with Warp. *Nat. Methods* **16**, 1146–1152 (2019).
92. Pettersen, E. F. et al. UCSF ChimeraX: Structure visualization for researchers, educators, and developers. *Protein Sci.* **30**, 70–82 (2021).
93. Schaible, G. A., Kohtz, A. J., Cliff, J. & Hatzenpichler, R. Correlative SIP-FISH-Raman-SEM-NanoSIMS links identity, morphology, biochemistry, and physiology of environmental microbes. *ISME Commun.* **2**, 52 (2022).
94. Fernando, E. Y. et al. Resolving the individual contribution of key microbial populations to enhanced biological phosphorus removal with Raman–FISH. *ISME J.* **13**, 1933–1946 (2019).
95. Majed, N. & Gu, A. Z. Application of Raman microscopy for simultaneous and quantitative evaluation of multiple intracellular polymers dynamics functionally relevant to enhanced biological phosphorus removal processes. *Environ. Sci. Technol.* **44**, 8601–8608 (2010).

Acknowledgements This study was funded through awards by the NASA Exobiology programme (80NSSC19K1633 to R.H.) and the Simons and the Gordon and Betty Moore Foundations (award 737750 to R.H.). M.P. was supported by the European Research Council (CoG 101000232) and the NOMIS foundation. A.J.K. was supported in part by the Thermal Biology Institute and MSU's Vice President's Office of Research, Economic Development and Graduate Education. V.K. was supported in part by a grant from the NSF (MCB-1817428 to R.H.). A portion of this research was performed under the Community Sciences Program (proposal https://doi.org/10.46936/10.25585/60008108) and used resources at the DOE Joint Genome Institute (https://ror.org/04xm1d337), which is a DOE Office of Science User Facility operated under contract no. DE-AC02-05CH11231. Raman imaging was made possible by The Center for Biofilm Engineering Imaging Facility at MSU, which is supported by funding from the NSF MRI program (2018562), the M. J. Murdock Charitable Trust (202016116), the US Department of Defense (77369LSRIP) and the Montana Nanotechnology Facility (an NNCI member supported by NSF grant ECCS-2025391). MSU's Confocal Raman microscope was acquired with support by the National Science Foundation (DBI-1726561) and the M. J. Murdock Charitable Trust (SR-2017331). We thank the US National Park Service for permitting work in YNP under permit number YELL-SCI-8010 and ScopeM for instrument access at ETH Zürich. We thank G. Chadwick for discussions on archaeal cell biology and physiology; L. Baranek for assistance with culture maintenance; C. Gauvin, A. Charbonneau and A. Kokhanovska for help with cryo-ET; M. Lynes for discussions that informed field sampling efforts; and M. Palmer for input on taxonomy. We thank W. Verstraete for allowing us to name this newly cultured methanogen after him.

Author contributions A.J.K. and R.H. developed the research project. A.J.K., V.K., N.P., M.P. and R.H. designed the experiments. A.J.K., V.K. and Z.J.J. conducted the field sampling. A.J.K. conducted cultivation, BONCAT, SIP, FISH, Raman and transcriptomic experiments, performed culture DNA and RNA extractions and phylogenetic analysis of hydrogenases. V.K. extracted DNA from LCB070 sediment, advised on cultivation and performed phylogenetic analysis of MCR sequences. Z.J.J. and A.J.K. analysed metagenomic data and performed phylogenetic analysis of genomes. A.J.K. performed the metabolic reconstruction with input from Z.J.J. and V.K. N.P. collected cryo-ET data. N.P. analysed cryo-ET data, with input from A.J.K., M.P. and R.H. R.H. and M.P. were responsible for funding and supervision of the project. A.J.K. and R.H. wrote the manuscript, which was then edited by all the authors.

Competing interests The authors declare no competing interests.

Additional information

Supplementary information The online version contains supplementary material available at https://doi.org/10.1038/s41586-024-07631-6.

Correspondence and requests for materials should be addressed to Roland Hatzenpichler.

Peer review information *Nature* thanks the anonymous reviewer(s) for their contribution to the peer review of this work.